HHS Public Access

Author manuscript

J Magn Reson Imaging. Author manuscript; available in PMC 2018 December 01.

Published in final edited form as:

J Magn Reson Imaging. 2017 December ; 46(6): 1748–1759. doi:10.1002/jmri.25712.

Computer-Aided Heterogeneity Analysis in Breast Magnetic Resonance Imaging Assessment of Ductal Carcinoma in Situ: Correlating Histologic Grade and Receptor Status

Shinn-Huey S. Chou, MD[1,2], **Eva C. Gombos, MD**[2], **Sona A. Chikarmane, MD**[2], **Catherine S. Giess, MD**[2], and **Jayender Jagadeesan, PhD**[2]

[1]Department of Radiology, Massachusetts General Hospital, 55 Fruit Street, Boston, MA 02114

[2]Department of Radiology, Brigham and Women's Hospital, 75 Francis Street, Boston, MA 02115

Abstract

Purpose—To identify breast magnetic resonance (MR) imaging biomarkers to predict histologic grade and receptor status of ductal carcinoma in situ (DCIS).

Materials and Methods—Informed consent was waived in this Health Insurance Portability and Accountability Act-compliant Institutional Review Board-approved study. Case inclusion was conducted from 7332 consecutive breast MR studies from 1/1/2009–12/31/2012. Excluding studies with benign diagnoses, studies without visible abnormal enhancement, and pathology containing invasive disease yielded 55 MR-imaged pathology-proven DCIS seen on 54 studies. Twenty-eight studies (52%) were performed at 1.5T; 26 (48%) at 3T. Regions-of-interest representing DCIS were segmented for pre-contrast, first and fourth post-contrast, and subtracted first and fourth post-contrast images on the open-source 3D Slicer software. Fifty-seven metrics of each DCIS were obtained, including distribution statistics, shape, morphology, Renyi dimensions, geometrical measure and texture, using the 3D Slicer HeterogeneityCAD module. Statistical correlation of heterogeneity metrics with DCIS grade and receptor status was performed using univariate Mann-Whitney test.

Results—Twenty-four of the 55 DCIS (44%) were high nuclear grade (HNG); 44 (80%) were estrogen receptor (ER) positive. Human epidermal growth factor receptor-2 (HER2) was amplified in 10/55 (18%), non-amplified in 34/55 (62%), unknown/equivocal in 8/55 (15%). Surface area-to-volume ratio showed significant difference ($p<0.05$) between HNG and non-HNG DCIS. No metric differentiated ER status ($0.113<p\leq1.000$). Seventeen metrics showed significant differences between HER2-positive and HER2-negative DCIS ($0.016<p<0.050$).

Conclusion—Quantitative heterogeneity analysis of DCIS suggests the presence of MR imaging biomarkers in classifying DCIS grade and HER2 status. Validation with larger samples and prospective studies is needed to translate these results into clinical applications.

Corresponding Author: Shinn-Huey S. Chou, MD, Department of Radiology, Massachusetts General hospital, 55 Fruit Street, Wang WAC-240, Boston, MA 02114, sschou@partners.org, Phone: 617-726-3093, Fax: 617-726-1074.

Keywords

Breast; Magnetic resonance imaging; Ductal carcinoma in situ; Computer-aided detection; Heterogeneity; Nuclear grade

INTRODUCTION

Ductal carcinoma in situ (DCIS), a pre-invasive form of breast cancer, is characterized by the proliferation of malignant epithelial cells confined by a myoepithelial layer (1). The term DCIS encompasses a variable spectrum of disease partly classified by its nuclear grade (low, intermediate, high) (1–3). Recent debates surrounding the optimal management of DCIS are based on the premise and data suggesting that high-grade DCIS progresses differently in its natural history and responds differently to treatment than low-grade DCIS (4,5). As such, active surveillance, rather than treatment, of low-grade DCIS has been proposed (6). Research trials exploring surveillance as an alternative management to surgery are also underway (7,8). Currently, the definitive diagnosis of DCIS must be confirmed by surgical excision because DCIS may harbor foci of invasive cancer incompletely sampled at core needle biopsy (9). It is the hope that magnetic resonance (MR) imaging aided by computer-aided detection (CAD) may help decipher some of the varied biological behavior of DCIS without or prior to definitive surgical intervention.

Dynamic contrast-enhanced (DCE) MR imaging is at present the most sensitive modality in the detection of breast cancer including DCIS (10–14). Research by Kuhl et al. indicates that contrast enhancement on MR imaging itself represents an imaging biomarker of DCIS with higher nuclear grade (14). Additionally, DCE MR imaging also allows for assessment of tumor heterogeneity, which can be quantified as phenotypic biomarkers of the disease (15). Heterogeneity analysis of breast cancer has been largely performed with ultrasound and MR imaging (15–22). Previous studies utilizing heterogeneity analysis in the development of MR imaging biomarkers focused on differentiating benign from malignant breast lesions and molecular subtypes of invasive breast cancer (22–24). Recent applications of heterogeneity analysis show promising results in the assessment of response of invasive breast cancer being treated with neoadjuvant therapy and the recurrence risk of invasive breast cancer (25–28).

Our aim was to identify MR imaging biomarkers that can predict the nuclear grade and receptor status of DCIS, thereby providing noninvasive insight into its diverse tumor biology with potential implications for future management.

MATERIALS AND METHODS

Case Selection

This study was Health Insurance Portability and Accountability Act-compliant and approved by our Institutional Review Board. Informed consent was waived given its retrospective design. Case selection was conducted from 7332 consecutive contrast-enhanced breast MR examinations (unilateral or bilateral) performed in 3864 women between January 1, 2009 and December 31, 2012. MR examinations with MR findings that subsequently underwent

histopathologic sampling were included in the study. Review of the electronic medical records further excluded patients without the diagnosis of DCIS, cases of DCIS showing invasive or microinvasive disease, and patients without final pathology from surgical excision internally reviewed by our breast pathologists. Applying these exclusion criteria yielded 93 patients with 94 cases of DCIS (one patient with bilateral DCIS). Among these, four more cases were excluded after correlating with the pathology reports: one case of DCIS focally involving a papilloma; one case of carcinoma in situ with equivocal classification between DCIS and pleormophic lobular carcinoma in situ (LCIS); one case of DCIS comprising two distinct cytomorphologies (low and high grades) within the same specimen; one case of DCIS without specified location in the mastectomy specimen and could not be correlated with the MR findings.

Of the remaining 89 patients with 90 cases of DCIS, 35 patients had MR imaging performed after surgical treatment and/or after prior biopsies without definitive residual enhancement. These 35 patients were excluded, yielding a final study population of 54 patients (all women) with 54 MR examinations showing 55 cases of DCIS; one woman had bilateral DCIS visualized on her MR examination (Table 1). Their ages at the time of diagnosis ranged from 26 to 79 with a median age of 49. No significant difference in age was found between 23/54 (43%) women with non-HNG DCIS and 31/54 (57%) women with HNG DCIS (p=0.22, Table 1). The woman with bilateral diseases had non-HNG DCIS in both breasts. Thirteen of the 55 cases of DCIS presented as residual enhancement on staging MR examinations after core biopsy diagnosis. Review of MR images and reports was performed by a breast-imaging fellow (S.S.C.) with the aid of a fellowship-trained radiologist with 12 years of breast MR imaging experience (E.C.G.).

Image Acquisition

Breast MR imaging during the study interval was acquired in prone position on a GE Signa 1.5T scanner with a four-channel GE dedicated breast surface coil (General Electric Healthcare, Milwaukee, WI) or a Siemens Trio 3T (Siemens Healthcare, Erlangen, Germany) scanner with a seven-channel dedicated breast surface coil (InVivo, Orlando, FL). From 2009 to 2012, 28 of the total 54 (52%) MR examinations were performed on a 1.5T scanner and the same number of examinations (28/54, 48%) was performed on a 3T scanner. DCE MR protocol included a three-plane localizing sequence, axial fat-suppressed T2-weighted fast spin-echo or short tau inversion recovery (STIR) sequence, axial T1-weighted gradient-echo sequence before contrast agent administration. Dynamic T1-weighted fat-suppressed 3D fast spoiled gradient-echo sequences were performed before and at four time points after intravenous injection of 0.1 mmol/kg of gadopentetate dimeglumine (Magnevist; Bayer, Whippany, NJ) with an average temporal resolution of ~90–100 seconds. Detailed parameters of the DCE 1.5T-MR protocol include 3D dynamically acquired pre- and post-contrast-enhanced T1-weighted fat-suppressed volumetric interpolated breath-hold examination (VIBE) sequences (12° flip angle, TR 6.1 msec, TE 2.9 msec, NEX 1.0, 300 × 300 mm field of view [FOV], 0.94 mm in-plane pixel resolution, 2.0/0.0 mm slice thickness/gap, acquisition time 1 min 36 sec per dynamic run). Detailed parameters of the DCE 3T-MR protocol include 3D dynamically acquired pre- and post-contrast-enhanced T1-weighted fat-suppressed VIBE sequences (8° flip angle, TR 4.6 msec, TE 1.6 msec, NEX 1.0, 340 ×

340 mm FOV, 0.76 mm in-plane pixel resolution, 2.0/0.0 mm slice thickness/gap, acquisition time 1 min 45 sec per dynamic run). Dynamic images were acquired in the sagittal plane before 2010 and in the axial plane during/after 2010; delayed imaging was performed in the plane orthogonal to dynamic imaging. Sagittal image acquisition prior to 2010 utilizes similar imaging parameters as the above-mentioned 1.5T-MR protocol, using sagittally acquired volume imaging for breast assessment (VIBRANT) dynamic series (2.0 mm slice thickness, acquisition time 1 min 36 sec). Post-processing was routinely applied, including image subtraction, maximum intensity projection, and computer-aided detection (CADstream; Sectra, Linkoping, Sweden, or VersaVue; iCAD, Nashua, NH).

MR Features Data Collection

Each MR examination was prospectively interpreted and given a final BI-RADS assessment by a radiologist specialized in breast imaging (29). Original radiology reports of all 54 MR examinations were reviewed by a breast-imaging fellow (S.S.C.) with the aid of a fellowship-trained radiologist with 12 years of breast MR imaging experience (E.C.G.). Data on MR features of the DCIS were extracted retrospectively from the radiology reports. Degree of background parenchymal enhancement (BPE) – minimal, mild, moderate, and marked, and amount of fibroglandular tissue (FGT) – fatty, scattered, heterogeneous, and extreme, were assigned prospectively based on the BI-RADS MR lexicon (29). MR findings of the DCIS were interpreted prospectively as focus, mass, or non-mass enhancement (NME) based on the lesion enhancement type according to the BI-RADS classification (29). Images of all 54 MR examinations were reviewed by the same breast-imaging fellow and fellowship-trained radiologist to verify that the recorded MR features correspond to the biopsy-proven DCIS.

Quantitative Analysis

The Digital Imaging and Communications in Medicine (DICOM) data of all 54 MR examinations were uploaded into an open-source image-processing and navigation software, 3D Slicer (Boston, MA). A breast-imaging fellow (S.S.C.) segmented the regions of interest (ROIs) on all slices semi-automatically based on the Otsu thresholding method, using the subtracted fourth post-contrast images (30). The subtracted fourth post-contrast images were co-registered with the pre-contrast, first and fourth post-contrast, and subtracted first post-contrast images on 3D Slicer, thereby simultaneously providing the ROIs on the pre-contrast and other post-contrast sequences when segmentation was performed on the subtracted fourth post-contrast images. The 55 ROIs outlined the region of enhancement representing the 55 cases of DCIS. Each ROI was visually verified and/or manually edited by the breast-imaging radiology fellow (S.S.C.).

The 3D image volume and label map that defined the ROIs were inputted into an open-source software module, HeterogeneityCAD (Boston, MA) (31), in 3D Slicer. The module quantified the heterogeneity of each ROI based on 57 metrics (31). The metrics were categorized as first-order statistics, shape and morphology, texture, geometry, and Renyi dimensions (31). First-order statistics included intensity values, skewness, variance, and kurtosis. Given that the signal intensity values did not take into consideration the MR transmitter gain, filter, and normalization process, percentages enhancement of the first and

fourth post-contrast sequences based on mean intensity values were calculated and included as one of the metrics. Shape and morphological metrics included volume, surface area, compactness, and maximum 3D diameter. Texture metrics derived from gray-level co-occurrence matrix (GLCM) and gray-level run-length (GLRL) matrix quantified texture coarseness. Renyi dimensions, a generalization of fractal and box-counting dimension, were computed under the assumption that each ROI was a fractal. Complete description and definitions of the metrics with more in-depth references are available online at https://www.slicer.org/wiki/Documentation/Nightly/Modules/HeterogeneityCAD (31). In total for each ROI, 57 numeric metric values were generated for each of its five imaging sequences: pre-contrast images, first post-contrast images, fourth post-contrast images, subtracted first post-contrast images, and subtracted fourth post-contrast images.

Histologic Assessments

DCIS grades ranged from low, low-to-intermediate, intermediate, intermediate-to-high, and high grade in the pathology reports. They were dichotomized into high-nuclear-grade (HNG, including intermediate-to-high and high-grade) DCIS and non-HNG (including low, low-to-intermediate, and intermediate) DCIS, as categorized in published relevant studies (7,32). Pathology reports of all specimens from core biopsy and surgical excisions were reviewed to confirm the worst pathologic assessment of each lesion. Estrogen receptor (ER) and progesterone receptor (PR) statuses were routinely tested on all DCIS at its initial diagnosis. Immunohistochemistry (IHC) stain for human epidermal growth factor receptor-2 (HER2) amplification in DCIS was routinely performed at our institution. However, no further analysis such as in-situ hybridization was pursued when HER2 IHC results were equivocal. Presence of calcifications and necrosis was documented in the pathology reports and collated.

Statistical Analysis

Clinical data such as patient demographics, MR descriptors, and DCIS features were compared between HNG and non-HNG DCIS using Student's t-test and Chi-square test. Statistical correlation of heterogeneity metrics with DCIS grade, ER status, and HER2 status, was performed using the univariate Mann-Whitney test, as the metrics were assumed to be non-normally distributed. Statistical correlation of heterogeneity metrics with DCIS nuclear grade was performed once more after exclusion of purely intermediate-grade DCIS from the non-HNG DCIS group to further dichotomize nuclear grades into low-grade (low and low-to-intermediate) versus high-grade (intermediate-to-high and high) DCIS. All statistical calculations were conducted with the statistical computing language R (version 3.2.4; R Foundation for Statistical Computing, Vienna, Austria), with statistical significance defined as $p < 0.05$.

RESULTS

MR Descriptors

Just over a quarter of the 54 MR examinations (n=14/54, 26%) were performed for the purpose of routine high-risk screening; majority of examinations (n=40/54, 74%) were obtained for diagnostic indications without a significant difference between the two groups

of women with non-HNG versus HNG DCIS (p=0.12, Table 1). There was no significant difference in the time period during which the MR examinations were obtained between the non-HNG and HNG groups (p=0.20, Table 1). In addition, the field strengths (1.5T vs. 3T scanners) of the MR examinations did not demonstrate any statistically significant difference between the non-HNG and HNG groups (p=0.43).

Seven of 24 (30%) MR examinations in the non-HNG group had moderate or marked BPE, compared to 14 of 31 (45%) in the HNG group (p=0.42, Table 1). Fifteen of 24 (65%) MR examinations in the non-HNG group had heterogeneous or extreme amount of fibroglandular tissue, compared to 24 of 31 (77%) in the HNG group (p=0.54). Therefore, no significant differences were noted in the degree of BPE and the amount of fibroglandular tissue on MR examinations between the non-HNG and HNG groups.

DCIS Features

Among the 55 cases of DCIS, 24 (44%) were non-HNG and 31 (56%) were HNG (Table 1). The sizes of the DCIS on MR imaging ranged from 6.0 mm to 133.8 mm with a mean size of 32.7 mm. There was no significant difference in size between the non-HNG and HNG groups (p=0.76). Majority (n=44/55, 80%) of the DCIS presented as NME on MR imaging; among them were 17 (71%) of the 24 non-HNG DCIS and 27 (87%) of the 31 HNG DCIS. Except for a single case of an enhancing focus (n=1/55, 2%), which represented non-HNG DCIS, the remaining cases presented as masses (n=10/55, 18%) – including 6 (25%) of the 24 non-HNG DCIS and 4 (13%) of the 31 HNG DCIS. There was no significant difference in the MR imaging lesion types between the non-HNG and HNG groups (p=0.24).

All of the non-HNG disease stained positive for ER and none were positive (IHC 3+) for HER2 amplification (Table 1). In contrast, 20 of 31 (65%) of the HNG cases were ER positive and nearly a-third (10/31, 32%) of HNG cases showed positive HER2 amplification. There were only a total of five confirmed triple negative/basal-like cases, all of which were HNG DCIS. The differences in the percentages of ER and HER2 positivity between non-HNG and HNG groups were statistically significant ($p \leq 0.001$).

Heterogeneity Correlation with DCIS Grade, ER Status, and HER2 Amplification

The voxel counts of the 55 ROIs ranged from 32 to 54,393, with a median of 365. Figures 1 and 2 demonstrated two sample cases of non-HNG and HNG DCIS, respectively, with the color-mapped ROIs representing enhancing disease on the post-contrast sequences.

One metric, surface-to-volume ratio, showed a significant difference between non-HNG and HNG DCIS on pre-contrast, first post-contrast, fourth post-contrast, and subtracted first post-contrast images (Table 2). Three heterogeneity metrics approached statistically significant differences between non-HNG and HNG disease on the subtracted fourth post-contrast images: Surface-volume ratio, low gray-level run emphasis (LGLRE), and short run low gray-level run emphasis (SRLGLE) (Table 3). The results of selective important metrics, including those that demonstrate and approach statistical significance, are summarized in box plots for the first post-contrast sequence (Figure 3A) and the fourth post-contrast sequence (Figure 3B). After excluding the purely intermediate-grade DCIS (n=10) from the non-HNG group to compare the low nuclear grade (LNG, n=14; low and low-to-

intermediate grade) versus HNG groups, the same single metric, surface-to-volume ratio, remained significantly different for the same MR sequences (Table 3). On the other hand, excluding intermediate-grade cases increased the total number of heterogeneity metrics that approached significant differences ($p<0.1$) between LNG and HNG DCIS to seven. These seven metrics included four additional metrics: Minimal intensity, skewness, kurtosis, and correlation (Table 3).

No metrics showed statistical significance in differentiating ER positive from ER negative DCIS, whereas multiple metrics were found significantly different between HER2 positive and HER2 negative disease (Table 2).

In detail, five metrics on the pre-contrast images, seven metrics on the first post-contrast images, two metrics on the fourth post-contrast images, ten metrics on the subtracted first post-contrast images, and two metrics on the subtracted fourth post-contrast images were significantly different between DCIS with and DCIS without HER2 amplification (Table 2). In total, 17 of 57 significant metrics were identified in the heterogeneity analysis of HER2 positive versus HER2 negative DCIS (Table 2). These metrics include short run emphasis (SRE), which was significantly different in all five imaging sequences – pre-contrast, first and fourth post-contrast, and subtracted first and fourth post-contrast sequences, and five additional metrics (minimum intensity, median intensity, mean deviation, standard deviation, and variance) that were significantly different in at least two of the five imaging sequences (Table 2). Percentage enhancement did not show significant differences between HER2 positive versus HER2 negative DCIS (Table 2).

DISCUSSION

In recent years, applications of heterogeneity analysis have demonstrated the potential of MR imaging biomarkers in improving the specificity of breast MR and providing clinically relevant biological indicators of invasive breast cancers (22–28). Until now, heterogeneity analysis has not been utilized in the development of MR imaging biomarkers of DCIS. Our study investigates the technique of computer-aided heterogeneity analysis in the characterization of DCIS and suggests the presence of MR imaging biomarkers in classifying DCIS nuclear grade and HER2 status.

Slightly more than half of our cases were intermediate-to-high-grade or high-grade DCIS, corroborating prior work by Kuhl and colleagues, which showed a greater sensitivity of MR imaging in the detection of intermediate and high-grade DCIS compared to mammography and increased sensitivity of MR imaging in the detection of DCIS with higher nuclear grade (14). HNG DCIS carries important prognostic impact, as they tend to progress more frequently and rapidly to invasive cancer that are more likely high grade (2,33). HNG DCIS also appears to respond differently to treatment compared to its low-grade counterpart (4,5).

None of the MR imaging parameters and descriptors that were analyzed showed a significant difference between HNG and non-HNG DCIS. MR BI-RADS lexicons that describe enhancement morphology – mass, NME, and focus – did not significantly differ between HNG and non-HNG DCIS. Additionally, heterogeneity metrics that represented

conventional size assessments by imaging, such as maximum 3D diameter, voxel count, and volume did not show any significant correlation with DCIS grade or receptor status. These findings were in accordance with prior research. Previously, Esserman and colleagues demonstrated that the combination of tumor distribution and enhancement characteristics on MR imaging reflected the underlying histopathology of DCIS (34). Yet, no significant correlation was identified between any single imaging variable with either nuclear grade or proliferative index, Ki67 (34). These results suggested that our current unaided visual perception and interpretation of MR imaging is inadequate to decode the biological variability of DCIS. Computer-aided heterogeneity analysis could therefore provide objective, quantitative, higher level imaging biomarkers to supplement existing knowledge and this current paper adds important information to this investigation.

Nonetheless, only one heterogeneity metric, surface-to-volume ratio, was significantly different between HNG and non-HNG DCIS. On average, HNG DCIS has a smaller surface-to-volume ratio than non-HNG disease. The biological basis and implication of this metric is unclear. A smaller surface-to-volume ratio would indicate that HNG DCIS is more compact, more consolidated, and higher in pixel density on imaging. Previous work revealed that pathologic tumor density significantly correlated with MR imaging density (34). As such, we could speculate that this metric depicts the tightly packed rapid expansion and overgrowth of HNG DCIS, in contrast with the more porous, non-contiguous, gradual spread of non-HNG DCIS. Interestingly, a total of 17 metrics showed significant differences between HER2 positive and HER2 negative diseases. Among these metrics, short-run emphasis was significantly greater in value for HER2 negative DCIS compared to HER2 positive disease across all five MR sequences. A short run-length consists of few consecutive pixels of the same gray-level intensity in a particular direction (35). Fine texture is populated by shorter runs (35). Therefore, a greater measure of short-run emphasis indicated an overall finer texture of HER2 negative DCIS relative to HER2 amplified disease. Four metrics analyzing signal intensity values – minimal, maximum, mean, and median intensity – showed an average lower pixel intensity in HER2 positive DCIS compared to HER2 negative disease. However, these values did not take into consideration the transmitter gain, filter, or undergo normalization. As such, percentage enhancement represents a more meaningful imaging biomarker, as it is normalized with respect to the absolute signal intensity of the pre-contrast images from the same examination and potentially reflects angiogenesis related to HER2 amplification, where observation of a relationship between MR imaging enhancement and the microvascular pattern of DCIS has been previously described (36). Positive association of HER2 amplification with periductal neovascularization has also been reported (37). Nevertheless, we found no statistically significant correlation of percentage enhancement with HER2 amplification status. Currently, HER2 amplification is not routinely tested in DCIS because its clinical or prognostic relevance is not yet elucidated (38,39). HER2 amplification is strongly associated with HNG, and as mentioned above, HNG DCIS is independently associated with increased recurrence and progression to invasive disease (2,33,38).

Two thirds of the imaging biomarkers that correlated with HER2 amplification were identified on the first post-contrast or subtracted first post-contrast sequences. This finding is revealing given that DCIS tends to demonstrate persistent enhancement kinetics and

therefore, DCIS often enhances most intensely on the delayed (fourth) post-contrast images. Yet only three metrics were identified on the fourth or subtracted fourth post-contrast sequences. These results emphasize the importance of the initial (first) post-contrast sequence, which likely presents the most accurate manifestation of the underlying pathophysiology for possibly both invasive cancers and DCIS. Interestingly, five of the 17 metrics were shown on the pre-contrast images. This observation suggests that non-contrast imaging potentially contains more information than we traditionally perceive.

Limitations of this study include its retrospective methodology and small sample size. Additionally, thirteen of the 55 cases (23.6%) of DCIS were biopsied prior to MR imaging, which could have affected some of the imaging metrics. A couple of reasons may have contributed to the lack of additional biomarkers in differentiating nuclear grades. The study may have been underpowered to detect significance in the remaining metrics. Alternatively, the binary classification of HNG and non-HNG groups may not be biologically relevant or appropriate. To address this possible explanation, we reclassified the nuclear grades into the LNG and HNG groups by excluding the intermediate-grade DCIS. We had hoped that the more biologically distinct separation of the two groups in terms of nuclear grades would identify more imaging biomarkers from heterogeneity analysis. The results showed the same single significant metric in differentiating nuclear grade, although more metrics approached statistical significance after the LNG versus HNG subdivision. This finding suggests that with larger sample sizes, these imaging metrics could demonstrate significant associations in differentiating LNG from HNG DCIS.

Similar explanations could account for the lack of correlation of heterogeneity metrics with ER status. Larger studies with a more enriched population of ER negative DCIS may unveil significant metrics. Our study had only five cases of confirmed triple negative/basal-like DCIS. With a larger sample, analysis based on luminal versus basal-like molecular subtypes may be more biologically relevant. As expected, ER negativity, HER2 amplification, and presence of necrosis correlated with HNG in the study.

Our univariate comparisons presented important exploratory results, which will require further validation with additional patients given that the heterogeneity features are high dimensional. While mathematical and imaging analytical definitions of the heterogeneity metrics have been well described (31), potential underlying biologic or pathophysiologic significance of these features requires further illumination. Future work with larger populations that allow for correlation with molecular subtypes and Oncotype DX DCIS scores is expected. Correlation of imaging heterogeneity features with long-term outcomes such as invasive recurrence may be achievable with much larger data sets. Based on the established MR imaging biomarkers, a machine-learning algorithm could then be developed to prospectively assess or predict the underlying DCIS tumor biology.

In conclusion, our study illustrates the feasibility and potential value of the use of computer-aided heterogeneity analysis in evaluating DCIS. Identification of MR imaging biomarkers helps increase the prognostic value of DCE MR imaging and may ultimately provide a non-invasive means to better understand the variable biological behavior of DCIS.

Acknowledgments

Grant Support: NIH National Institute of Biomedical Imaging and Bioengineering P41EB015898 and NIH National Center for Research Resources P41RR019703

References

1. Virnig BA, Tuttle TM, Shamliyan T, Kane RL. Ductal carcinoma in situ of the breast: a systematic review of incidence, treatment, and outcomes. Journal of the National Cancer Institute. 2010; 102:170–178. [PubMed: 20071685]
2. Leonard GD, Swain SM. Ductal carcinoma in situ, complexities and challenges. Journal of the National Cancer Institute. 2004; 96:906–920. [PubMed: 15199110]
3. Consensus Conference on the classification of ductal carcinoma in situ. The Consensus Conference Committee. Cancer. 1997; 80:1798–1802. [PubMed: 9351550]
4. Narod SA, Iqbal J, Giannakeas V, Sopik V, Sun P. Breast Cancer Mortality After a Diagnosis of Ductal Carcinoma In Situ. JAMA oncology. 2015; 1:888–896. [PubMed: 26291673]
5. Sagara Y, Mallory MA, Wong S, et al. Survival Benefit of Breast Surgery for Low-Grade Ductal Carcinoma In Situ: A Population-Based Cohort Study. JAMA surgery. 2015; 150:739–745. [PubMed: 26039049]
6. Esserman L, Yau C. Rethinking the Standard for Ductal Carcinoma In Situ Treatment. JAMA oncology. 2015; 1:881–883. [PubMed: 26291410]
7. Francis A, Thomas J, Fallowfield L, et al. Addressing overtreatment of screen detected DCIS; the LORIS trial. European journal of cancer (Oxford, England: 1990). 2015; 51:2296–2303.
8. Elshof LE, Tryfonidis K, Slaets L, et al. Feasibility of a prospective, randomised, open-label, international multicentre, phase III, non-inferiority trial to assess the safety of active surveillance for low risk ductal carcinoma in situ - The LORD study. European journal of cancer (Oxford, England: 1990). 2015; 51:1497–1510.
9. Brennan ME, Turner RM, Ciatto S, et al. Ductal carcinoma in situ at core-needle biopsy: meta-analysis of underestimation and predictors of invasive breast cancer. Radiology. 2011; 260:119–128. [PubMed: 21493791]
10. Berg WA, Zhang Z, Lehrer D, et al. Detection of breast cancer with addition of annual screening ultrasound or a single screening MRI to mammography in women with elevated breast cancer risk. JAMA: the journal of the American Medical Association. 2012; 307:1394–1404. [PubMed: 22474203]
11. Lehman CD, Isaacs C, Schnall MD, et al. Cancer yield of mammography, MR, and US in high-risk women: prospective multi-institution breast cancer screening study. Radiology. 2007; 244:381–388. [PubMed: 17641362]
12. Sardanelli F, Podo F, D'Agnolo G, et al. Multicenter comparative multimodality surveillance of women at genetic-familial high risk for breast cancer (HIBCRIT study): interim results. Radiology. 2007; 242:698–715. [PubMed: 17244718]
13. Lehman CD. Magnetic resonance imaging in the evaluation of ductal carcinoma in situ. Journal of the National Cancer Institute Monographs. 2010; 2010:150–151. [PubMed: 20956821]
14. Kuhl CK, Schrading S, Bieling HB, et al. MRI for diagnosis of pure ductal carcinoma in situ: a prospective observational study. Lancet. 2007; 370:485–492. [PubMed: 17693177]
15. Alic L, Niessen WJ, Veenland JF. Quantification of heterogeneity as a biomarker in tumor imaging: a systematic review. PloS one. 2014; 9:e110300. [PubMed: 25330171]
16. Chen SJ, Cheng KS, Dai YC, et al. Quantitatively characterizing the textural features of sonographic images for breast cancer with histopathologic correlation. Journal of ultrasound in medicine: official journal of the American Institute of Ultrasound in Medicine. 2005; 24:651–661. [PubMed: 15840797]
17. Alvarenga AV, Infantosi AF, Pereira WC, Azevedo CM. Assessing the combined performance of texture and morphological parameters in distinguishing breast tumors in ultrasound images. Med Phys. 2012; 39:7350–7358. [PubMed: 23231284]

18. Ardakani AA, Gharbali A, Mohammadi A. Classification of breast tumors using sonographic texture analysis. Journal of ultrasound in medicine: official journal of the American Institute of Ultrasound in Medicine. 2015; 34:225–231. [PubMed: 25614395]
19. Moon WK, Huang YS, Lo CM, et al. Computer-aided diagnosis for distinguishing between triple-negative breast cancer and fibroadenomas based on ultrasound texture features. Med Phys. 2015; 42:3024–3035. [PubMed: 26127055]
20. Chaudhury B, Zhou M, Goldgof DB, et al. Heterogeneity in intratumoral regions with rapid gadolinium washout correlates with estrogen receptor status and nodal metastasis. Journal of magnetic resonance imaging: JMRI. 2015; 42:1421–1430. [PubMed: 25884277]
21. Ko ES, Kim JH, Lim Y, Han BK, Cho EY, Nam SJ. Assessment of Invasive Breast Cancer Heterogeneity Using Whole-Tumor Magnetic Resonance Imaging Texture Analysis: Correlations With Detailed Pathological Findings. Medicine. 2016; 95:e2453. [PubMed: 26817878]
22. Chang RF, Chen HH, Chang YC, Huang CS, Chen JH, Lo CM. Quantification of breast tumor heterogeneity for ER status, HER2 status, and TN molecular subtype evaluation on DCE-MRI. Magnetic resonance imaging. 2016; 34:809–819. [PubMed: 26968141]
23. Karahaliou A, Vassiou K, Arikidis NS, Skiadopoulos S, Kanavou T, Costaridou L. Assessing heterogeneity of lesion enhancement kinetics in dynamic contrast-enhanced MRI for breast cancer diagnosis. The British journal of radiology. 2010; 83:296–309. [PubMed: 20335440]
24. Sutton EJ, Oh JH, Dashevsky BZ, et al. Breast cancer subtype intertumor heterogeneity: MRI-based features predict results of a genomic assay. Journal of magnetic resonance imaging: JMRI. 2015; 42:1398–1406. [PubMed: 25850931]
25. Ahmed A, Gibbs P, Pickles M, Turnbull L. Texture analysis in assessment and prediction of chemotherapy response in breast cancer. Journal of magnetic resonance imaging: JMRI. 2013; 38:89–101. [PubMed: 23238914]
26. Wu J, Gong G, Cui Y, Li R. Intratumor partitioning and texture analysis of dynamic contrast-enhanced (DCE)-MRI identifies relevant tumor subregions to predict pathological response of breast cancer to neoadjuvant chemotherapy. Journal of magnetic resonance imaging: JMRI. 2016
27. Michoux N, Van den Broeck S, Lacoste L, et al. Texture analysis on MR images helps predicting non-response to NAC in breast cancer. BMC cancer. 2015; 15:574. [PubMed: 26243303]
28. Li H, Zhu Y, Burnside ES, et al. MR Imaging Radiomics Signatures for Predicting the Risk of Breast Cancer Recurrence as Given by Research Versions of MammaPrint, Oncotype DX, and AM50 Gene Assays. Radiology. 2016:152110.
29. Morris, EACC., Lee, CH., et al. ACR BI-RADS® Atlas, Breast Imaging Reporting and Data System. Reston, VA: American College of Radiology; 2013. ACR BI-RADS® Magnetic Resonance Imaging.
30. Otsu N. A threshold selection method from gray-level histograms. IEEE Trans Syst Man Cybernet. 1979; 9:62–66.
31. Narayan, V., Jaynder, J. HeterogeneityCAD module in 3D Slicer. https://http://www.slicer.org/slicerWiki/index.php/Documentation/Nightly/Modules/HeterogeneityCAD. Updated 22 March 2016. Accessed 19 July 2016
32. Rahbar H, Partridge SC, Demartini WB, et al. In vivo assessment of ductal carcinoma in situ grade: a model incorporating dynamic contrast-enhanced and diffusion-weighted breast MR imaging parameters. Radiology. 2012; 263:374–382. [PubMed: 22517955]
33. Lagios MD. Heterogeneity of duct carcinoma in situ (DCIS): relationship of grade and subtype analysis to local recurrence and risk of invasive transformation. Cancer Lett. 1995; 90:97–102. [PubMed: 7720048]
34. Esserman LJ, Kumar AS, Herrera AF, et al. Magnetic resonance imaging captures the biology of ductal carcinoma in situ. J Clin Oncol. 2006; 24:4603–4610. [PubMed: 17008702]
35. Nailon, W. Youxin, Mao, editor. Texture Analysis Methods for Medical Image Characterisation. BiomedicalImaging. 2010. InTech, Available from: http://www.intechopen.com/books/biomedical-imaging/texture-analysis-methods-for-medical-image-characterisation
36. Santamaria G, Velasco M, Farrus B, Caparros FX, Fernandez PL. Dynamic contrast-enhanced MRI reveals the extent and the microvascular pattern of breast ductal carcinoma in situ. The breast journal. 2013; 19:402–410. [PubMed: 23758454]

37. Claus EB, Chu P, Howe CL, et al. Pathobiologic findings in DCIS of the breast: morphologic features, angiogenesis, HER-2/neu and hormone receptors. Experimental and molecular pathology. 2001; 70:303–316. [PubMed: 11418009]

38. Poulakaki N, Makris GM, Battista MJ, et al. Hormonal receptor status, Ki-67 and HER2 expression: Prognostic value in the recurrence of ductal carcinoma in situ of the breast? Breast (Edinburgh, Scotland). 2016; 25:57–61.

39. Lari SA, Kuerer HM. Biological Markers in DCIS and Risk of Breast Recurrence: A Systematic Review. Journal of Cancer. 2011; 2:232–261. [PubMed: 21552384]

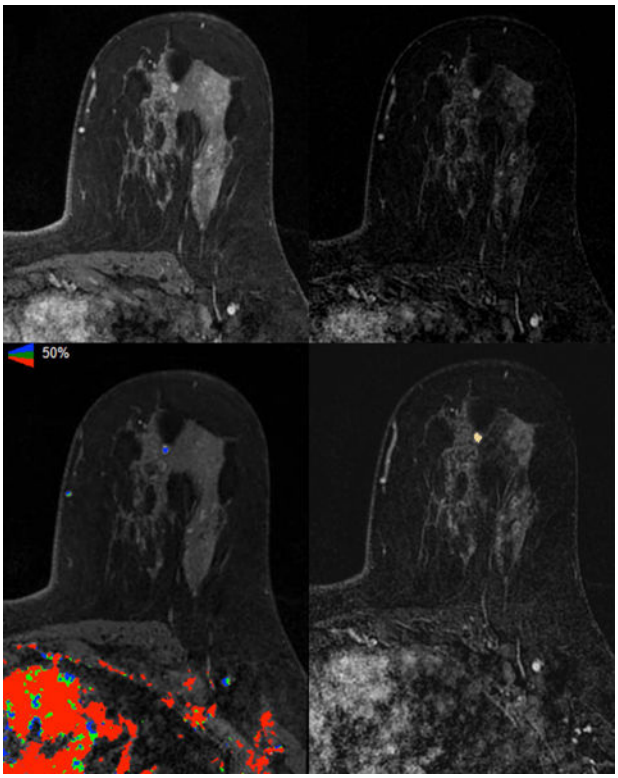

Figure 1.

Axial images of A) T1 fat-suppressed fourth post-contrast sequence, B) subtracted fourth post-contrast sequence, C) iCAD color registration of the subtracted first post-contrast subtraction sequence, and D) 3D Slicer segmentation of the subtracted fourth post-contrast sequence showed a 6 mm irregular mass in the left upper breast of a 36-year-old woman with a known contralateral invasive cancer (not shown); excision showed ER positive and HER2 negative intermediate-grade DCIS.

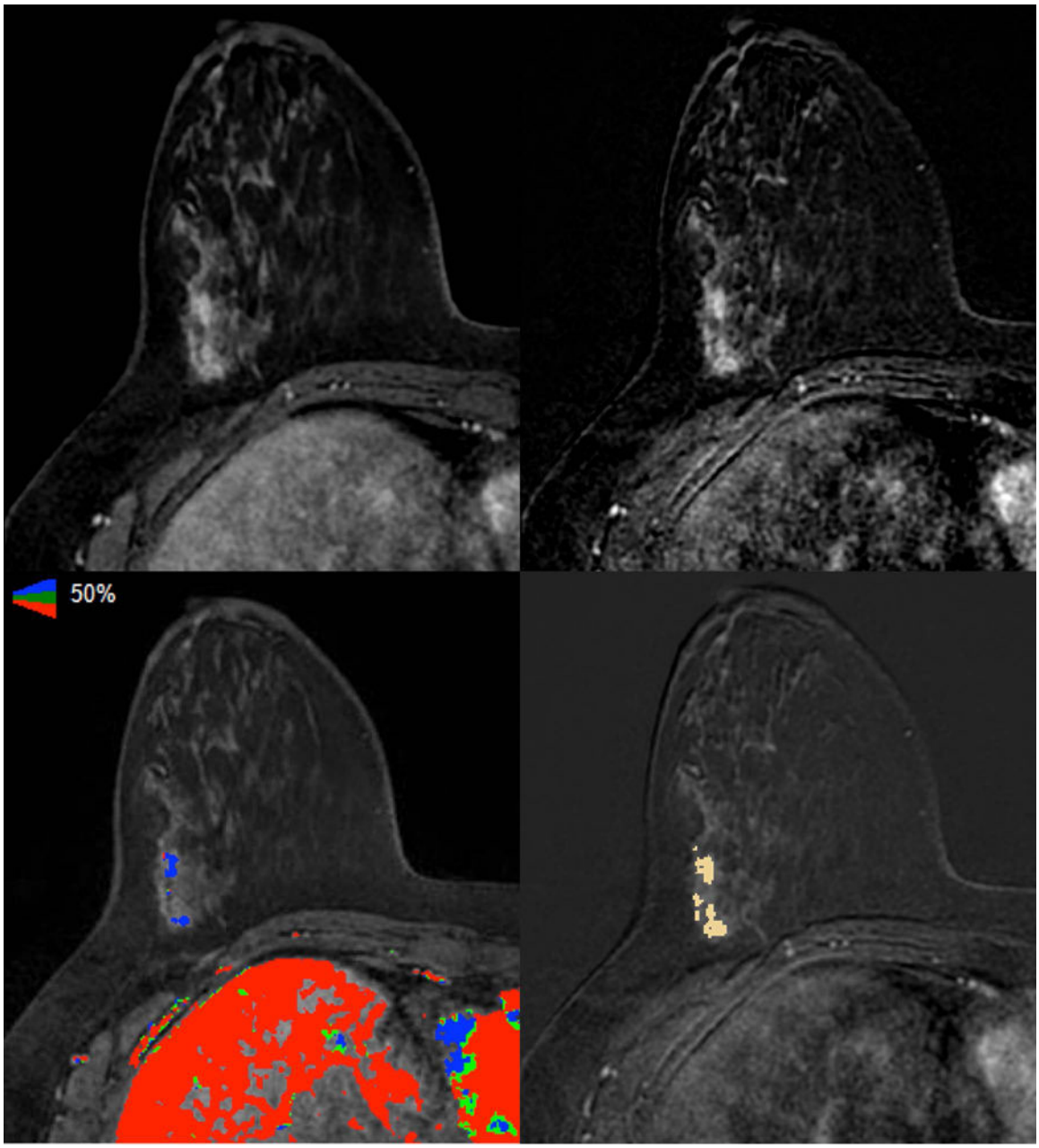

Figure 2.

Axial images of A) T1 fat-suppressed fourth post-contrast sequence, B) subtracted fourth post-contrast sequence, C) iCAD color registration of the first subtracted post-contrast sequence, and D) 3D Slicer segmentation of the subtracted fourth post-contrast sequence showed linear non-mass enhancement (NME) in the right lateral breast of a 48-year-old woman with a known contralateral invasive cancer (not shown); excision showed ER positive and HER2 equivocal high-grade DCIS.

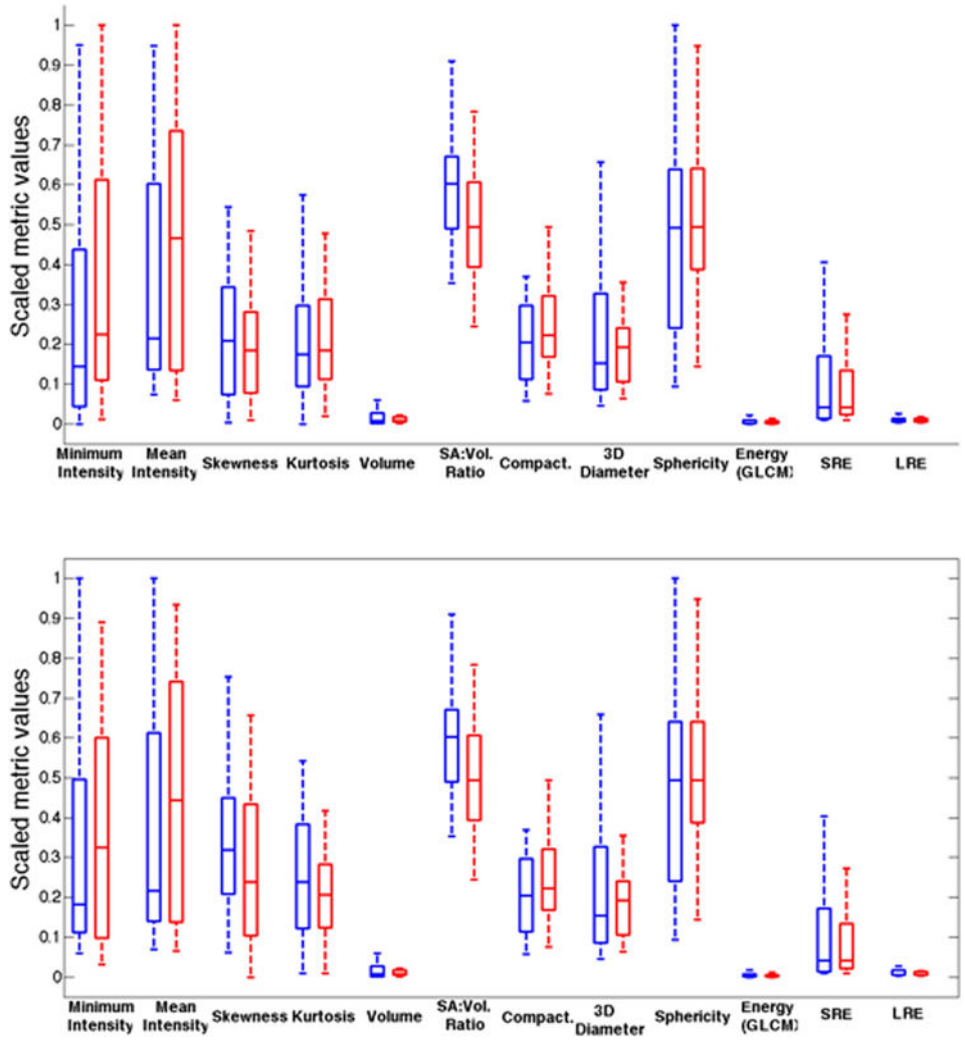

Figure 3.

Box plots showing representative metrics for non-high nuclear grade (non-HNG; blue) and HNG (red) DCIS based on the (A) first post-contrast sequence and the (B) fourth post-contrast sequence.

Table 1

Patient demographics, MR parameters, imaging descriptors, and DCIS features in association with DCIS nuclear grades.

Characteristics		Non-HNG, N(%) or Median [range] or Mean±stdev	HNG, N(%) or Median [range] or Mean±stdev	Total, N(%) or Median [range] or Mean±stdev
Patient Demographics (N=54)				
	Female	23	31	54 (100)
	Age (yr)	49 [34–79]	54 [26–77]	49 [26–79]
				$p = 0.22$
MR Examinations (N=54)				
Exam indication	Screening	3 (13)	11 (35)	14 (26)
	Diagnostic	20 (87)	20 (65)	40 (74)
				$p = 0.12$
Year	2009	10 (43)	8 (26)	18 (33)
	2010	4 (17)	14 (45)	18 (33)
	2011	5 (22)	5 (16)	10 (19)
	2012	4 (17)	4 (13)	8 (15)
				$p = 0.20$
Magnet strength (T)	1.5	10 (43)	18 (58)	28 (52)
	3	13 (57)	13 (42)	26 (48)
				$p = 0.43$
Degree of background parenchymal enhancement				
	Minimal/Mild	16 (70)	17 (55)	33 (61)
	Moderate/Marked	7 (30)	14 (45)	21 (39)
				$p = 0.42$
Amount of fibroglandular tissue				
	Fatty/Scattered	8 (35)	7 (23)	15 (28)
Heterogeneous/Extreme		15 (65)	24 (77)	38 (72)
				$p = 0.50$
DCIS Features (N=55)				
Grade		24	31	55
Size (mm)		34.1 ± 32.8	31.6 ± 25.9	32.7 ± 28.9
				$p = 0.76$
MR lesion type	NME	17 (71)	27 (87)	44 (80)
	Mass	6 (25)	4 (13)	10 (18)
	Focus	1 (4)	0 (0)	1 (2)
				$p = 0.24$
Estrogen receptor	Positive	24 (100)	20 (65)	44 (80)
	Negative	0 (0)	11 (35)	11 (20)
				$p =$ **0.003**

Characteristics		**Non-HNG, N(%) or Median [range] or Mean±stdev**	**HNG, N(%) or Median [range] or Mean±stdev**	**Total, N(%) or Median [range] or Mean±stdev**
HER2	Positive	0 (0)	10 (32)	10 (18)
(n/a in 3)	Negative	21 (88)	13 (42)	34 (62)
	Equivocal	2 (8)	6 (19)	8 (15)
				p = **0.004**
Calcifications	Present	14 (58)	19 (61)	33 (60)
(n/a in 1)	Absent	9 (38)	12 (39)	21 (38)
				p = 0.52
Necrosis	Present	11 (46)	28 (90)	39 (71)
(n/a in 1)	Absent	12 (50)	3 (10)	15 (27)
				p = **0.001**

Table 2

Summary of MR imaging metrics with significant differences in nuclear grades and HER2 amplification of DCIS.

	Mean value ± standard deviation			Mean value ± standard deviation		
Metrics	**Non-HNG**	**HNG**	***p* value**	**HER2−**	**HER2+**	***p* value**
Minimum intensity						
Pre	117.2±137.2	152.9±163.3	0.396	155.9±156.7	45.6±52.3	**0.039**
4th Post	468±402.8	568.9±423.3	0.338	561.2±417.7	282.5±315.1	**0.050**
Maximum intensity						
Sub 1st Post	573.0±413.3	629.4±513.2	0.593	648.1±452.6	365.5±330.8	**0.048**
Mean intensity						
1st Post	618.0±488.9	763.6±529.1	0.423	748.7±520.9	384.1±376.7	**0.047**
Median intensity						
1st Post	618.5±489.7	752.1±518.1	0.464	747.6±519.8	380.8±374.1	**0.047**
Sub 1st Post	261.6±235.5	283.3±254.6	0.905	312.8±257.9	158.4±172.9	**0.048**
Percentage enhancement (based on Mean intensity)						
1st Post	80.60±35.92	79.72±24.42	0.768	81.54±34.88	74.47±14.03	0.629
4th Post	130.7±52.8	127.4±26.5	0.550	127.4±45.8	133.1±29.5	0.447
Range						
Sub 1st Post	525.8±355.2	570.2±459.3	0.605	581.3±385.7	327.8±271.7	**0.044**
Mean deviation						
1st Post	120.2±82.9	147.1±122.6	0.873	142.3±103.8	72.4±71.2	**0.028**
Sub 1st Post	86.4±59.2	94.59±88.63	0.539	98.4±70.1	50.2±45.5	**0.022**
Root mean square						
1st Post	637.0±497.2	786.4±546.3	0.423	771.0±532.6	394.9±386.5	**0.047**
Standard deviation						
1st Post	147.9±101.5	181.1±145.8	0.900	175.0±124.8	90.2±88.4	**0.022**
Sub 1st Post	104.6±70.8	116.4±104.8	0.619	119.4±83.3	63.2±58.6	**0.031**
Skewness						
Sub 1st Post	0.347±0.500	0.499±0.624	0.240	0.272±0.288	0.496±0.279	**0.031**

	Mean value ± standard deviation			Mean value ± standard deviation		
Metrics	**Non-HNG**	**HNG**	***p* value**	**HER2−**	**HER2+**	***p* value**
Kurtosis						
Sub 1st Post	−0.081±1.448	0.440±2.744	0.121	−0.368±0.600	0.028±0.394	**0.016**
Variance						
1st Post	31749±34150	53363±77983	0.900	45759±64973	15176±28067	**0.022**
Sub 1st Post	15753±18349	24188±40573	0.619	20986±26669	7087±11980	**0.031**
Surface : Volume ratio						
Pre	2.483±0.606	2.100±0.613	**0.027**	2.322±0.571	2.299±0.526	0.080
1st Post	2.482±0.607	2.098±0.614	**0.026**	2.321±0.571	2.291±0.532	0.080
4th Post	2.481±0.607	2.098±0.614	**0.026**	2.321±0.571	2.291±0.532	0.080
Sub 1st Post	2.643±0.780	2.183±0.608	**0.032**	2.399±0.607	2.301±0.525	0.085
Homogeneity 1						
Pre	184.4±578.4	121.8±391.8	0.341	130.9±489.6	302.2±667.3	**0.047**
Homogeneity 2						
Pre	82.0±248.6	63.1±216.2	0.423	57.43±210.5	163.8±370.3	**0.038**
Inverse variance						
Pre	86.2±260.5	66.0±224.7	0.395	60.68±220.6	170.3±385.1	**0.041**
Short run emphasis (SRE)						
Pre	0.841±0.117	0.819±0.113	0.528	0.846±0.111	0.750±0.098	**0.022**
1st Post	0.843±0.116	0.823±0.112	0.608	0.848±0.112	0.758±0.094	**0.041**
4th Post	0.842±0.116	0.823±0.112	0.608	0.847±0.111	0.757±0.095	**0.044**
Sub 1st Post	0.839±0.121	0.819±0.115	0.550	0.846±0.111	0.757±0.095	**0.044**
Sub 4th Post	0.840±0.118	0.819±0.114	0.573	0.846±0.111	0.756±0.095	**0.041**
Gray-level non-uniformity (GLN)						
Sub 1st Post	31.8±121.4	18.3±45.7	0.395	22.91±102.3	28.40±56.13	**0.047**
Long run low gray-level run emphasis (LRLGLE)						
Sub 4th Post	0.782±1.319	0.640±1.527	0.668	0.601±1.168	1.523±2.475	**0.019**

Table 3

Summary of MR imaging metrics with significant differences and metrics approaching significant differences in DCIS nuclear grades between non-high nuclear grade (non-HNG; low, low-to-intermediate, and intermediate) and high nuclear grade (HNG; intermediate-to-high and high) groups and between low nuclear grade (LNG; low and low-to-intermediate) and HNG groups.

	Mean value ± standard deviation			**Mean value ± standard deviation**		
Metrics	**Non-HNG**	**HNG**	***p* value**	**LNG**	**HNG**	***p* value**
Minimum intensity						
1st Post	236.5±258.9	323.3±278.9	0.169	186.1±223.2	323.3±278.9	0.088
Sub 1st Post	47.2±102.4	59.3±101.9	0.140	31.0±82.5	59.3±101.9	0.056
Skewness						
Sub 4th Post	0.950±0.520	0.817±0.318	0.269	1.092±0.527	0.817±0.318	0.084
Kurtosis						
Sub 4th Post	0.792±1.388	0.275±0.783	0.221	1.129±1.547	0.275±0.783	0.084
Surface : Volume ratio						
Pre	2.483±0.606	2.100±0.613	**0.027**	2.510±0.596	2.100±0.613	**0.042**
1st Post	2.482±0.607	2.098±0.614	**0.026**	2.509±0.598	2.098±0.614	**0.040**
4th Post	2.481±0.607	2.098±0.614	**0.026**	2.508±0.598	2.098±0.614	**0.040**
Sub 1st Post	2.643±0.780	2.183±0.608	**0.032**	2.748±0.848	2.183±0.608	**0.037**
Sub 4th Post	2.526±0.670	2.168±0.587	0.060	2.585±0.703	2.168±0.587	0.064
Correlation						
4th Post	1.3E7±3.2E7	2.1E7±4.6E7	0.130	1.8E7±4.1E7	2.1E7±4.6E7	0.098
Low gray-level run emphasis (LGLRE)						
Sub 4th Post	0.024±0.016	0.019±0.017	0.085	0.025±0.017	0.019±0.017	0.075
Short run low gray-level run emphasis (SRLGLE)						
Sub 4th Post	0.019±0.014	0.014±0.013	0.098	0.021±0.015	0.014±0.014	0.071

J Magn Reson Imaging. Author manuscript; available in PMC 2018 December 01.